ELSEVIER

Colloids and Surfaces A: Physicochem. Eng. Aspects 219 (2003) 215–231

COLLOIDS AND SURFACES A

www.elsevier.com/locate/colsurfa

A high-accuracy polynomial fitting approach to determine contact angles

A. Bateni [a], S.S. Susnar [a], A. Amirfazli [b], A.W. Neumann [a,*]

[a] *Department of Mechanical and Industrial Engineering, University of Toronto, 5 King's College Road, Toronto, Ont., Canada M5S 3G8*
[b] *Department of Mechanical Engineering, University of Alberta, Edmonton, Alta., Canada T6G 2G8*

Received 15 August 2002; accepted 23 January 2003

Abstract

An automated polynomial fitting (APF) scheme is presented for high-accuracy contact angle measurements. The APF method acquires highly magnified (e.g. 35×) images of a drop and extracts the drop profile using image processing techniques. Then a polynomial is fitted to the experimentally observed drop profile and the contact angle is calculated using the slope of the polynomial at the contact point. Different edge detection techniques were examined and it was found that the Laplacian of Gaussian edge detection method performs well for the highly magnified images. A thorough statistical analysis was carried out to determine the optimum parameters for the curve fitting e.g., the order of the polynomial and the number of pixels used in the fitting procedure. A comparison of the APF method with Axisymmetric Drop Shape Analysis (ADSA) indicates good agreement between the two methods. The APF method is applicable to a variety of situations, e.g., liquid lens systems, non-axisymmetric drops, and electrically charged drops, where application of traditional contact angle measurement methods may not be accurate enough.

Keywords: Contact angle; Drop shape; Polynomial fitting; Image processing; Surface tension

1. Introduction

The contact angle concept is of fundamental importance in all solid–liquid–fluid interfacial phenomena, such as wetting of solid surfaces, capillary penetration into porous media, and flotation. Moreover, contact angles can provide information about hydrophobicity of a surface, surface heterogeneity, surface roughness, solid surface energy, liquid surface tension, and line tension [1–7].

The Young's equation correlates the Young's contact angle, θ_Y, liquid–vapor surface tension, γ_{lv}, solid–vapor surface tension, γ_{sv}, and solid–liquid surface tension, γ_{sl}, as:

$$\cos\theta_Y = \frac{\gamma_{sv} - \gamma_{sl}}{\gamma_{lv}} \quad (1)$$

Using the Young's equation, one can obtain information about the solid and liquid surface tensions [1,5–9]. However, accurate measurement

* Corresponding author. Tel.: +1-416-978-1270; fax: +1-416-978-7753.
E-mail address: neumann@mie.utoronto.ca (A.W. Neumann).

0927-7757/03/$ - see front matter
doi:10.1016/S0927-7757(03)00053-0

and correct interpretation of the contact angle is crucial in any application of the Young's equation.

Due to the lack of mobility of the molecules in the solid surface, solid surface tensions cannot be measured directly [6]. Among the several independent approaches developed to estimate solid surface tensions, the contact angle measurement is believed to be the simplest and the most straightforward approach, and certainly has attracted many researchers [10–14]. Contact angles are quite sensitive to local changes in surface energies and topography; the measurement scheme presented here is of such accuracy that can be used as an ideal tool for the study of the surface energies and properties such as roughness and heterogeneity.

Contact angles of electrically charged drops are also of particular interest in many applications (e.g. electrostatic painting, electrostatic spraying, and ink-jet printing) and can provide information about liquid surface tensions in the electric field [15–19]. However, currently available Axisymmetric Drop Shape Analysis (ADSA) schemes are not valid when an electric field is present, and the conventional contact angle measurement methods are not accurate enough for this purpose (see below). This paper presents a methodology for contact angle measurement which is applicable to various situations, including presence of an electric field.

In spite of the conceptual simplicity, experience has shown that the acquisition of accurate, reliable, and thermodynamically significant contact angles requires painstaking effort. The accuracy of the results in contact angle measurements can be affected by the quality of solid surfaces, the purity of the measuring liquids, and the skill of the experimenter, but also by the methodology and procedure. Different methods have been developed for measuring contact angles [6,20–23,25–30]. The choice of a particular method depends on the geometry of the system as well as the materials involved and the thermodynamic state of the system. The contact angle of a sessile drop (or an adhering gas bubble) is often measured from the meridian profile of the drop/bubble. Currently, the most frequently used methods for contact angle measurement from a drop profile are the conventional goniometer method and advanced methods such as ADSA [6,20].

In the goniometer method the contact angle is measured simply by aligning a tangent to the drop profile at the point where the three interfaces meet (i.e. base of a drop). The contact angle of a liquid drop on a solid can be measured either directly using a telescope equipped with a goniometer eyepiece or from a photograph of the drop profile. The main drawback of the goniometer method is that it is subjective and the results depend on the experience of the operator. Although certain training procedures can be used to improve the reproducibility, the accuracy of the goniometer method is usually $\pm 2^{\circ}$ at best [6,20]. Moreover, the goniometer measurements may produce a mixture of thermodynamically meaningful and meaningless contact angles, with no criteria to distinguish between the two [9].

In the ADSA methodology an image of a drop is obtained and the drop profile is extracted using image processing techniques. The experimental drop shape is assumed to be Laplacian and axisymmetric. A theoretical curve described by the Laplace equation is fitted to the experimental profile. The contact angle is calculated from the slope of the theoretical curve at the contact point. Details of the methodology and the experimental setup can be found elsewhere [21–24].

ADSA has been widely used and has proved to produce accurate and reliable contact angles. The ADSA technique averages over small irregularities of experimental drops. Therefore, it may not be very sensitive to small changes in the contact angle caused by local surface heterogeneities and/or roughness. The method presented in this paper is free from such global averaging.

The currently available schemes of ADSA are not applicable to a number of cases e.g., in the presence of an electric field, non-axisymmetric drops, or liquid lens systems, which have been used to investigate line tensions and also the drop size dependence of contact angles [31]. Since no particular physical or geometrical assumption is made in the polynomial fitting method presented here, it can be applied to all of the above systems.

There are other schemes available which have attempted to improve the goniometer method by

putting a tangent to a drop profile using more advanced procedures (e.g. polynomial fitting methods). However, these methods often have shortcomings and more effort is required to provide statistically reliable schemes. To analyze the difficulties of such schemes we refer to our own work where a high-order polynomial fitting scheme with variable number of pixel points was produced [25]. In this scheme the drop profile coordinates were extracted from a digital image using the same image processing techniques as ADSA (i.e. Sobel edge detection technique). Then high-order polynomials were fitted to the profile coordinates on each side of the drop near contact points and the contact angle for each side was calculated as the slope of the polynomial at the contact point. In [25] the optimum number of coordinate points (i.e. the length of the profile) was chosen according to maximum correlation coefficient criteria. To verify the results, the profile was rotated 90° (i.e. the X and Y axes were reversed) and new polynomials were fitted to both sides of the profile, resulting in two other contact angles. Therefore, four contact angles were calculated for each sessile drop, which ideally should all be equal. However, it was realized that sometimes the calculated contact angles differ significantly from one side of the drop to the other side and also when the profile is rotated. Neglecting these discrepancies, the scheme developed by del Río et al. [25] showed relatively good agreement with the results of the ADSA method. Finally, del Río et al. concluded that producing a robust polynomial fitting scheme that would perform adequately under various experimental conditions is a task far from trivial, and circumspection is necessary in using the available schemes.

In this work we have improved upon shortcomings with the del Río's and similar other schemes. The high-order polynomials usually used are too sensitive to experimental noise causing a significant error in contact angle calculations. The order of the polynomial used in the fitting procedure plays an important role in the contact angle calculations; thus, a careful analysis is required to determine the optimum order of the polynomial (see below). The other area in the scheme presented in [25] that can be improved upon to compensate for its limited application is the number of pixels used in the fitting procedure. This was determined based on the maximum correlation coefficient criterion. It is shown in this paper that the correlation coefficient is not sensitive enough for this purpose. Thus, to obtain accurate contact angle results the optimum number of coordinate points should be calculated using other statistical methods (e.g. the standard error).

In this paper we address such deficiencies and present an automated, self-contained scheme based on a polynomial fitting approach, which produces high-accuracy measurements of contact angles. The APF scheme consists of two main modules: image processing and curve fitting. The methods which are used to determine the parameters of these modules are also explained. Experimentally, validation of the new polynomial fitting scheme is provided by comparing the results of this method with those of ADSA. Finally, the advantages and disadvantages of the polynomial fitting method are compared with the other contact angle measurements schemes.

2. Automated polynomial fitting methodology

Automated polynomial fitting (APF) measures contact angles by fitting a polynomial curve to the drop or meniscus meridian profile and calculating the slope of the curve at the contact point, where the three interfaces meet (Fig. 1).

The APF scheme consists of two main modules. The first module acquires an image of a drop and extracts the experimental drop profile using image analysis techniques. The second module fits a polynomial curve to a part of the experimental profile near the contact point and calculates the contact angle using the slope of the theoretical curve at the contact point. The APF experimental procedure is described below.

2.1. Image processing module

This module acquires images of a sessile drop (or bubble) and extracts the experimental drop profile as a series of coordinate points, which will

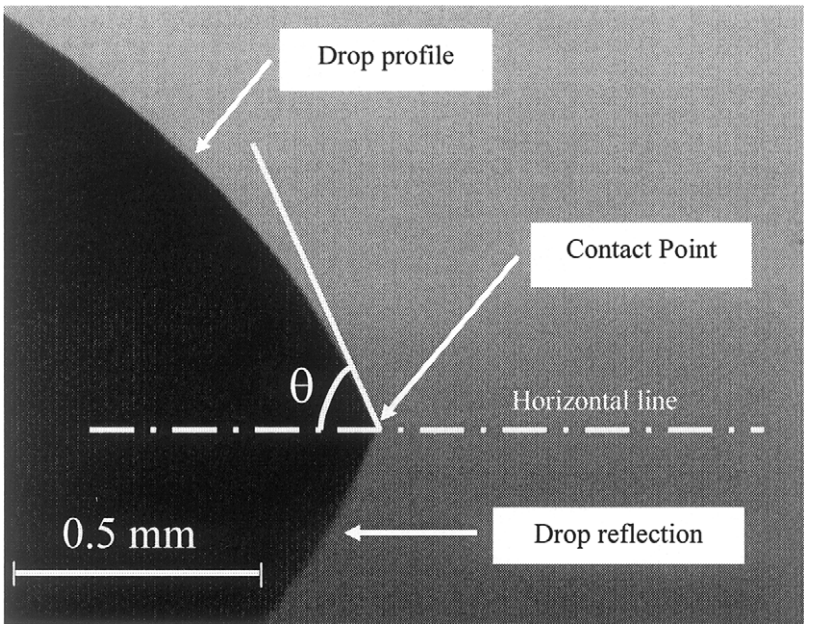

Fig. 1. Image of the right side of a sessile drop of water on a PMMA surface; magnification: 35 × . The cusp angle is the result of the reflection of the drop image at the solid surface.

be sent, as an input, to the curve fitting module of the scheme. Highly magnified images (e.g. 35 ×) are used in the current version of the APF scheme (Fig. 1). Since the whole drop profile would not fit into a magnified image, images are taken from the right or left contact point of the drop (Fig. 1). Highly magnified images are preferred for the following reasons.

(1) Considering the fact that the drop profile far from the contact point has little information about the contact angle, inclusion of a large portion of the drop profile in the fitting procedure reduces the sensitivity of the scheme for the actual contact angle. Highly magnified images, which are taken from the contact point, provide maximum information about this area and thus the contact angle.

(2) Since in a highly magnified image each pixel represents a smaller physical area than at lower magnification, the error caused by the digital resolution of the image will be smaller, compared to the usual low magnification (e.g. 5 ×).

(3) Magnified profiles have smaller curvature and can be better described by low order polynomials. Application of low order polynomials (e.g. third-order) are preferred because they are less sensitive to experimental noise and produce more stable results (see below).

The MATLAB[1] R12 Image Processing Toolbox has been used to study different edge detection methods. Preliminary tests have shown that the edge detection of highly magnified digital images (used in the APF method) is more complicated than that of regular low magnification ones (Figs. 2 and 3). In this analysis, a typical high magnification image was selected and several edge detection methods, i.e., Canny, Sobel, Prewitt, and Laplacian of Gaussian (LOG) were employed to extract the drop profile from the digital image (Fig. 4). The results clearly indicate that Sobel and Prewitt methods are not appropriate for the high magnification images. Close inspection of the profiles generated by the Canny and LOG methods shows that the Canny profile is not as smooth as the profile generated by the LOG method (Fig. 5). Also there are some discontinuities in the profile detected by the Canny method, which would cause difficulties in profile extraction and curve fitting

[1] MATLAB is a registered trade mark of MathWorks, Inc.

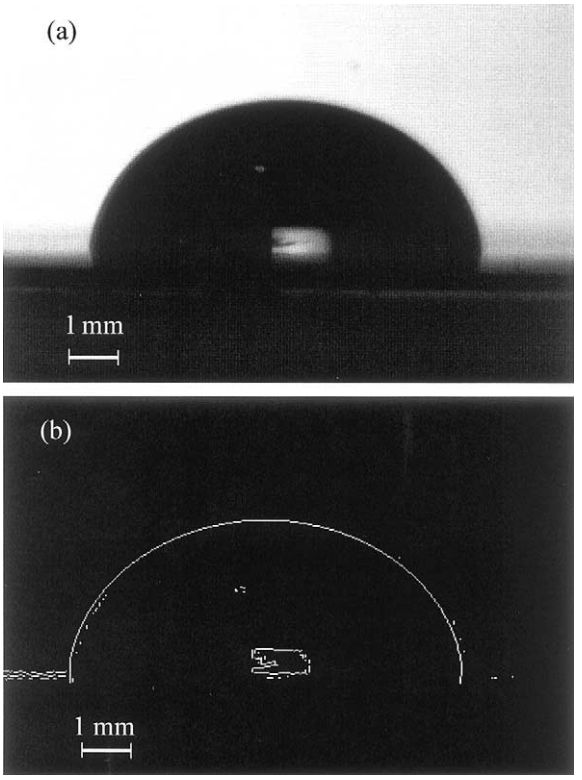

Fig. 2. (a) A typical low magnification (ADSA type) image. (b) The result of the default edge detection (Sobel) method of the MATLAB R12 Image Processing Toolbox.

procedure. Therefore, it is concluded that LOG is the most suitable technique to extract drop profiles from high magnification digital images. In this method, first the image is blurred using a Gaussian filtering, and then the edges are detected using a Laplacian technique. The noise observed in the Figures after edge detection will be removed by the APF program.

To optimize the quality/accuracy of the detected profiles the following two parameters of the LOG scheme needed to be adjusted: the sensitivity threshold parameter and the standard deviation parameter for filtering. Fig. 6 shows that a high filtering parameter will produce less noise, i.e., a cleaner profile. To ensure that the filtering process does not affect the real drop profile (and consequently the contact angle, θ) the APF program was run for several different parameter sets. The results indicate that when θ is less than 90° the filtering procedure does not affect the measured contact angle (Fig. 7a). However, when θ is larger than 90° filtering may have a significant effect on the results (Fig. 7b). It was also found that a smaller sensitivity parameter is needed when the filtering parameter was increased. Therefore, for the former case higher values of the filtering parameter (e.g. 4.0) and a small value of the sensitivity parameter (e.g. 0.0001) were used; and for the latter case ($\theta > 90$) the default value of the filtering parameter (i.e. 2.0) and a sensitivity parameter of 0.01 were used.

2.2. Curve fitting module

Using the extracted drop profile, the APF scheme automatically determines whether the image is taken from the right or left side of the drop. Then it detects the pixel that represents the drop contact point. For sessile drops, the contact point can be simply defined as the pixel with the local maximum or minimum value of the X coordinate depending on whether the image is from the right or left side and whether the contact angle, θ, is higher or lower than 90°. For instance, for an image taken from the right side of the drop and when $\theta < 90$, the contact point is the pixel with the maximum X coordinate (Fig. 8). In other applications of the APF method, such as liquid lens systems, the contact point can be determined as the pixel point at which a sharp change in the slope of the profile is observed.

In the next step, a series of P coordinate points are selected next to the contact point and a polynomial of the order O is fitted to the selected pixels (Fig. 9). This polynomial can be expressed as

$$Y_{\text{polynomial}} = \sum_{i=0}^{O} a_i x^i \tag{2}$$

The $O+1$ coefficients of the polynomial, a_i, are calculated using the least-squares algorithm, which results in the best fit of the polynomial curve to the experimental pixel points. Then, the contact angle, θ, is computed from the first derivative of the polynomial at the contact point, i.e.

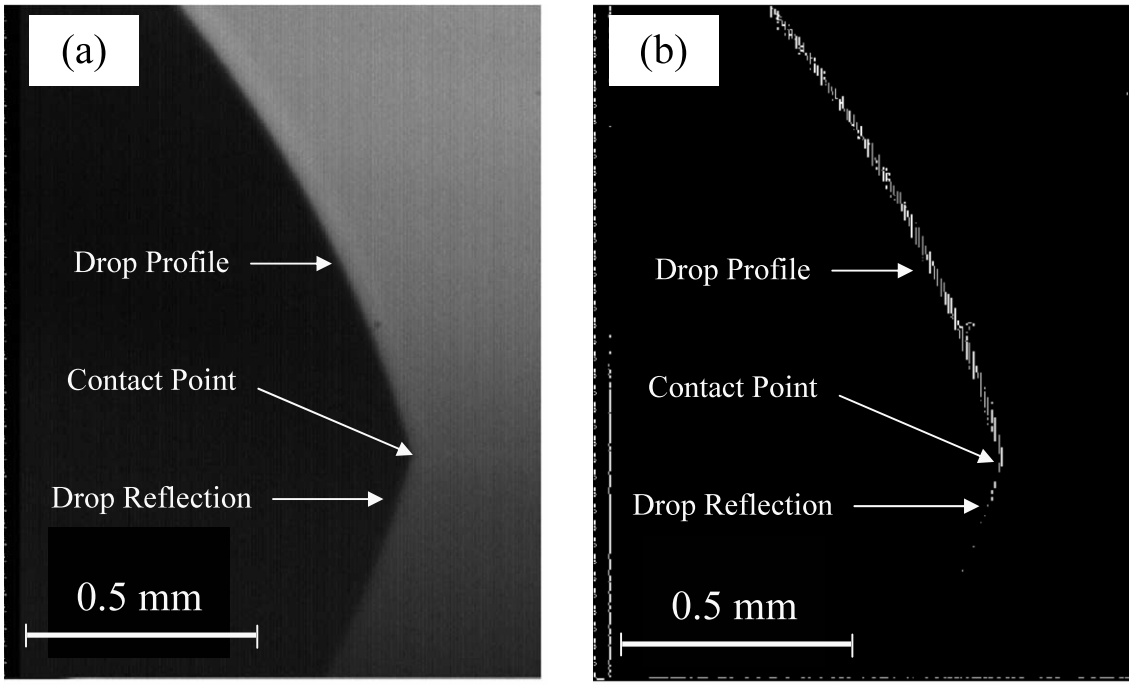

Fig. 3. The edge of a high magnification image cannot be detected by the default edge detection (Sobel) method of MATLAB. (a) A typical high magnification (APF type) image. (b) The result of the default edge detection method of the MATLAB R12 Image Processing Toolbox (Sobel method). The detected edge does not form a curve to be considered as a drop profile (note the series of vertical lines in frame b).

$$\theta = \mathrm{abs}\left[\tan^{-1}\left(\frac{\mathrm{d}Y_{\mathrm{poynomial}}}{\mathrm{d}x}\right)_{X_{\mathrm{contact}}}\right] \quad \text{(3-a)}$$

for $\theta < 90$

$$\theta = \mathrm{abs}\left[\tan^{-1}\left(\frac{\mathrm{d}Y_{\mathrm{poynomial}}}{\mathrm{d}x}\right)_{X_{\mathrm{contact}}}\right] + 90 \quad \text{(3-b)}$$

for $\theta > 90$

Two main parameters should be assigned for the APF program, i.e., the order of the polynomial, O, and the number of pixels to be considered in the curve fitting procedure, P. Preliminary tests have shown that these parameters have a significant effect on the calculation of contact angles, thus a thorough analysis was performed to evaluate the optimum values.

The above two parameters should be analyzed simultaneously because of the strong correlation between them, i.e., higher order polynomials require more pixel coordinates (see below). Moreover, because of the noise in an experimental image, a polynomial curve that fits one drop profile is not necessarily the best for all images. Hence, the analysis should be based on the average result obtained from a statistically significant number of images.

Several experiments were performed with sessile drops of water on polymethyl methacrylate (PMMA) surfaces and a series of images were obtained from both sides of the drop. The experimental images were processed by the APF program with several different combinations of the parameters P and O (i.e. $P = 10, 20, 30, \ldots, 260$ and $O = 1, 2, 3, 4, 5, 6$). The analysis is limited to 260 pixels and the sixth-order polynomials because of limitation in the length of the profiles (i.e. each drop profile at $35\times$ magnification consists of $\approx$ 260 pixels). Several criteria used to evaluate the best combination of the parameters P and O are discussed in the following section.

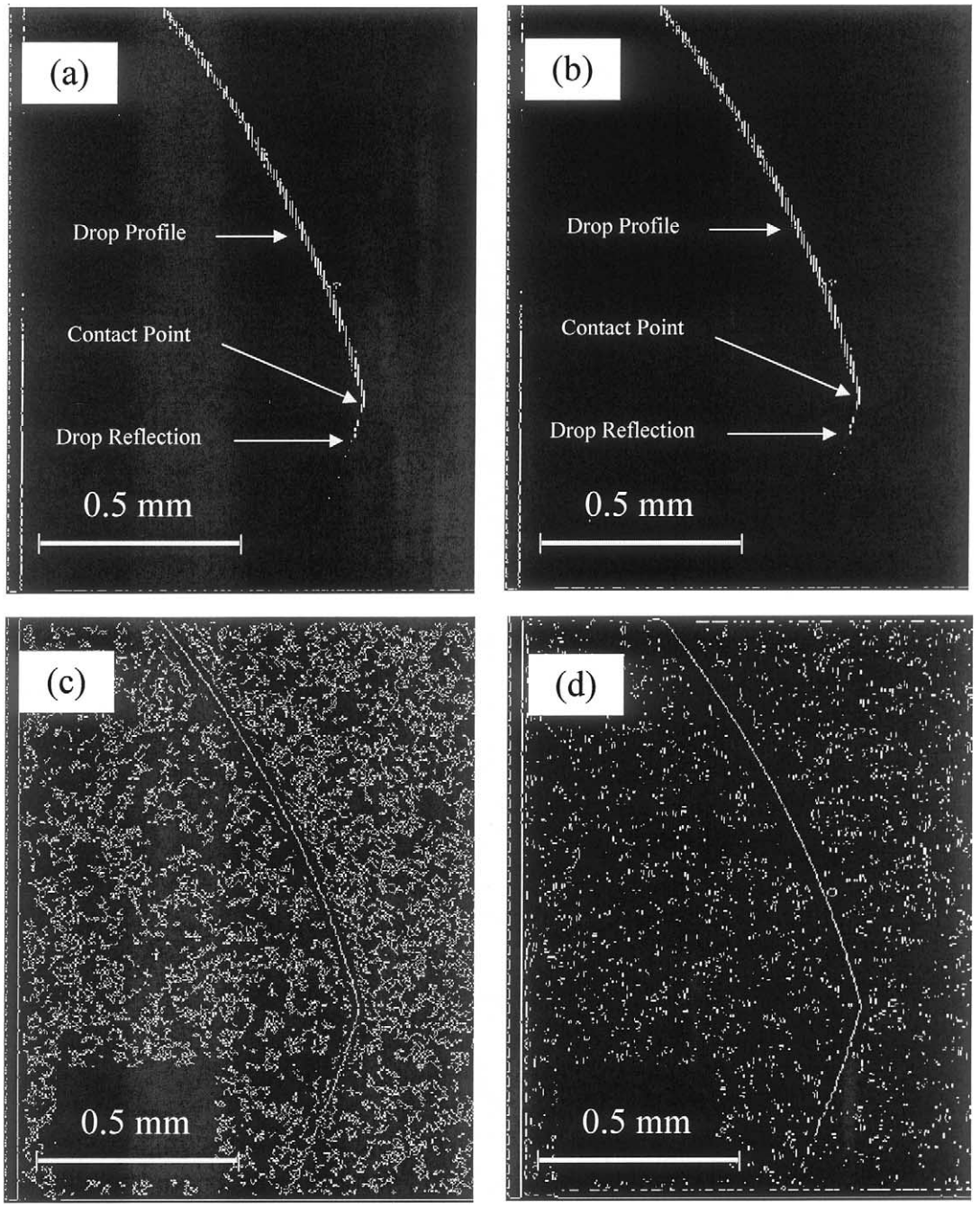

Fig. 4. Comparison of different edge detection methods for high magnification images. (a) The Sobel edge detection technique. The method has failed to detect the drop profile as a smooth curve. (b) The Prewitt edge detection technique. The method has failed to detect the drop profile as a smooth curve. (c) The Canny edge detection technique. The method detects the drop profile, but there is significant noise in the background. (d) The LOG edge detection technique. This method performs better than the other edge detection methods for high magnification images.

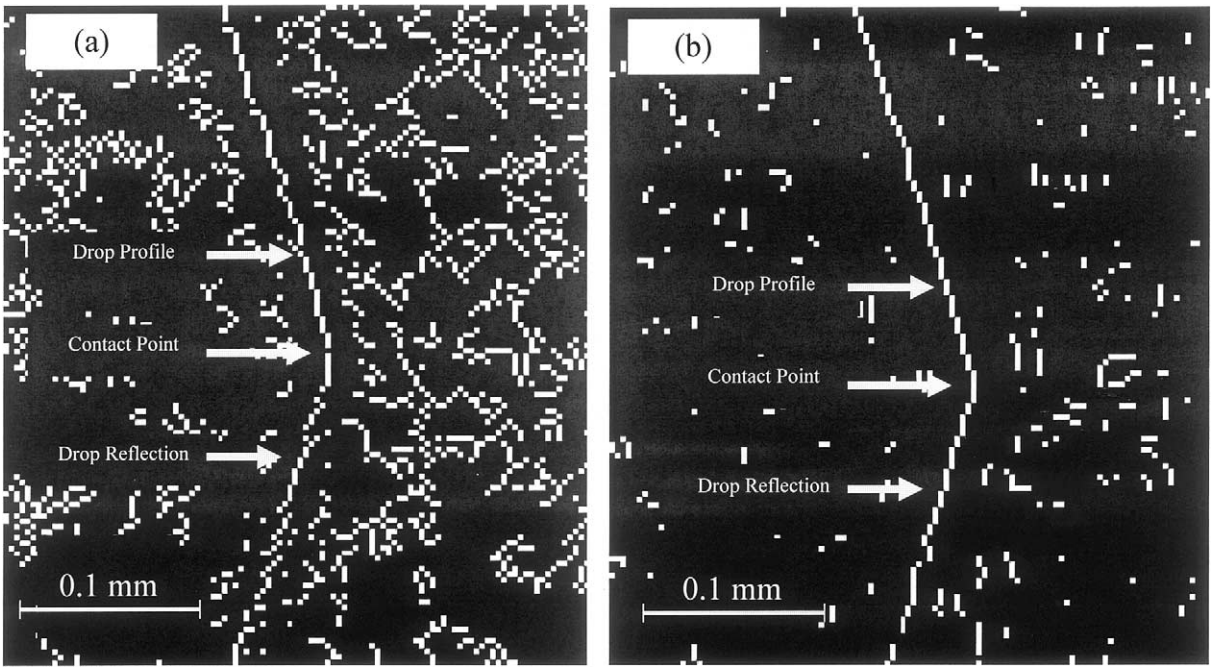

Fig. 5. (a) Magnified view of the detected edge by the Canny edge detection method. (b) Magnified view of the detected edge by the LOG edge detection method. The magnified views shows that the Canny profile is not smooth and has some discontinuities. On the other hand the LOG method produces smooth curves within the pixel resolution limits of the image. Therefore, LOG is the preferred edge detection method for high magnification images.

2.2.1. The stability of the results

The first criterion used for selecting the parameters P and O is the stability of the calculated contact angle, i.e., the results should not be too sensitive to the parameters. In order to examine the stability of the results, the average contact angles were plotted versus the number of pixels, P, for each polynomial (Fig. 10).

Fig. 10 shows that a first-order polynomial (i.e. linear regression) is very sensitive to the parameter P. When P is small ($P < 25$), the measured contact angle increases with increasing number of pixels, then there is a short stable area around $P = 30$, and finally the contact angle decreases with increasing P. This pattern seems reasonable because for $P < 25$ the number of pixels is too small to be fitted to any kind of polynomial (see Fig. 11a), and for $P > 35$ the linear fit cannot account for the curvature of the profile (see Fig. 11b). Therefore, it is concluded that the appropriate number of pixels for the first-order fit should be around 30; however, in general the linear fit is too sensitive to the number of pixels and is not suitable (very narrow stable band compared to higher order polynomials, see Fig. 10).

A similar pattern is observed for higher order polynomials. The calculated contact angle increases with increasing number of pixels, then there is a stable area, and finally it decreases for high values of P. It is also observed that more pixels are needed to obtain a stable result from higher order polynomials (see Fig. 12).

Among the polynomials considered in Fig. 11, the polynomial with the third-order has a wider stability area than others. Therefore, according to this analysis the third-order polynomial with 120–140 pixels is an appropriate combination to be used in the APF method. We need a statistical

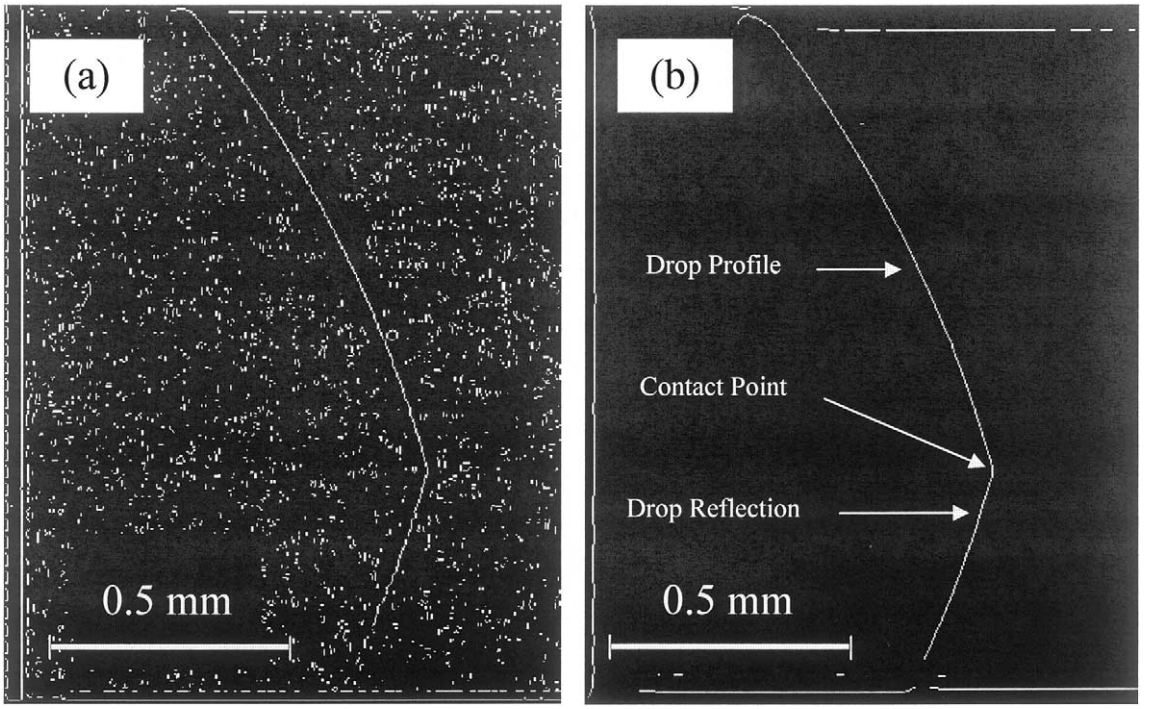

Fig. 6. The effect of the filtering parameter of the LOG method. (a) The result of the LOG method when the sensitivity parameter is 0.001 and the filtering parameter is 2.0 (default parameters). (b) The sensitivity parameter is 0.0001 and the filtering parameter is 6.0. The noise in the background is reduced by using higher filtering parameters.

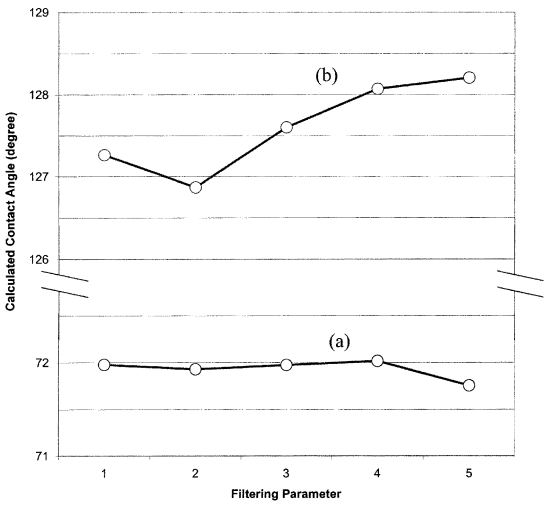

Fig. 7. The effect of the filtering process on contact angles calculated by the APF method. (a) Water on PMMA coated silicon wafer (contact angle $< 90^\circ$). (b) Water on Teflon coated silicon wafer (contact angle $> 90^\circ$).

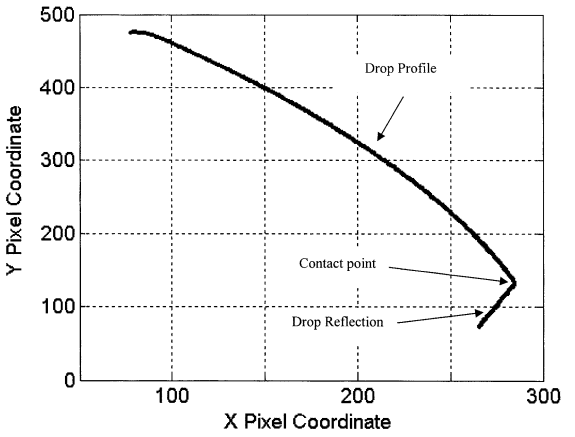

Fig. 8. The detected profile of a sessile drop with contact angle $< 90^\circ$. The contact point is defined as the pixel with maximum X coordinate.

measure to substantiate our observations further; usually, the correlation coefficient is used for this purpose.

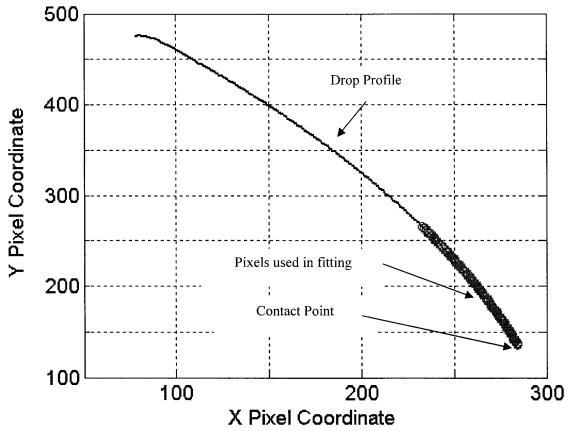

Fig. 9. A series of 130 pixel points next to the contact point is selected to be fitted in a polynomial curve. The selected pixels represent a length of about 0.5 mm along the drop profile.

2.2.2. The correlation coefficient

The correlation coefficient (R^2) is a statistical tool that is often used to evaluate how well a theoretical curve can describe experimental observations. The R^2 is defined as

$$R^2 = \frac{\sum_i (Y_{\text{polynomial}} - \bar{Y}_{\text{profile}})_i^2}{\sum_i (Y_{\text{profile}} - \bar{Y}_{\text{profile}})_i^2} \quad (5)$$

Higher correlation coefficients (close to one) imply better representation of the experimental observations. The R^2 was calculated by the APF program for every image obtained in the experiments. The averages of the calculated R^2 are graphed versus the number of pixels P, for of the O-th order polynomials (Fig. 13).

Fig. 13 shows that for each polynomial the correlation coefficient increases to a value very close to one, then there is a stable area (the flat region), and finally it decreases as the value of P is increased. In general, the behavior of R^2 is similar to the stability of the calculated contact angles discussed earlier; and the maximum R^2 occur at the same area that the stable results were observed in Fig. 10. The R^2 values at the stability area are very close to one which indicates that the polynomials fit the extracted profile very well. How-

Fig. 10. Average contact angle for several polynomials of different order versus number of pixels. Each of the sections between the vertical gridlines represents a different polynomial (first-order to sixth-order); and the horizontal axis shows the number of pixels (10, 20,. . .,260) used in the fitting procedure.

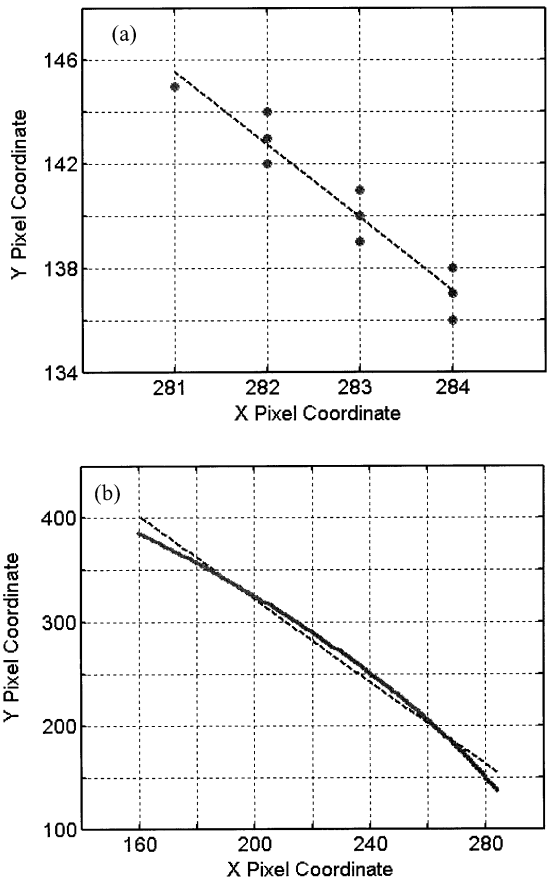

Fig. 11. A first order polynomial (dashed line) is fitted to the drop profile. (a) The circles represent the detected pixels signifying drop edge ($P = 10$). Adding or removing a pixel will change the slope of the line significantly, i.e., the calculated contact angle is sensitive to the number of pixels, P. (b) The solid line represent the detected drop profile ($P = 250$). The graph clearly shows that a first order polynomial cannot account for the curvature of the profile when P is large.

ever, it seems that the correlation coefficients are not sensitive enough to be used as a criterion for choosing P and O values. For example, for the second-order polynomial the R^2 is almost constant for the area of $P \in (80, 180)$, while during the same interval the measured contact angle is changing a few degrees. As a result, an additional criterion should be used to evaluate the suitability of the fitted curves to the experimental profile.

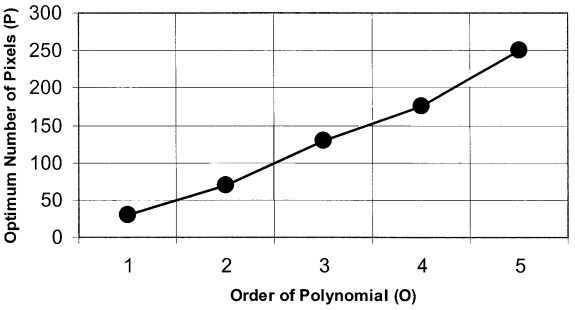

Fig. 12. The optimum number of pixels needed for the APF's fitting module increases with increasing order of the polynomial used.

2.2.3. The standard error

Another statistical tool that can be used to evaluate a curve fitting procedure is the standard error, which is given by [32]

$$S = \sqrt{\frac{\sum_{j}^{P} (Y_{\text{polynomial}} - Y_{\text{profile}})_j^2}{P - (O + 1)}} \tag{6}$$

where j refers to the j-th pixel of the profile. The standard errors were calculated by the APF program for each image of the experiment. The average of the standard error is graphed versus the number of pixels P, for each of the O-th order polynomials (see Fig. 14). Fig. 14 shows that the standard error is relatively small and stable for small P. Then it increases with increasing number of pixels. The Figure also indicates that the minimum standard error is almost equal for different orders of the polynomials (i.e. ~ 0.8). This criterion can be used to determine the optimum number of pixels when the order of the polynomial is determined, e.g., it indicates that 130 pixels represent the best fit for third-order polynomials.

2.2.4. Selecting the optimum values of P and O

Considering all of the above criteria it is concluded that the third-order polynomial with 130 pixels will produce stable results with high correlation coefficient and small standard error. The fourth-order polynomials also have the same R^2 and standard error, and produce the same

Fig. 13. Average correlation coefficient for several polynomials of different order versus number of pixels. Each of the sections between the vertical gridlines represents a different polynomial (first-order to sixth-order); and the horizontal axis shows the number of pixels (10, 20,. . .,260) used in the fitting procedure.

contact angle results as the third-order polynomials. However, the third-order polynomial has a wider stable area and is preferred. Higher order polynomials (e.g. fifth-order or sixth-order) are not appropriate because they are more sensitive to experimental noise. Moreover, the high magnification images used in the APF method do not provide enough pixel points to be fitted to higher order polynomials.

3. Results and validation

To validate the APF scheme, several experiments were performed with both ADSA and APF using different materials and the results were compared. Details of the experimental procedures for low-rate dynamic contact angle measurements (used for the ADSA method) were described elsewhere [21–24]. Similar procedures have been used for the APF method except that highly magnified images (e.g. 35 × compared to 6 × for ADSA) were obtained from the contact area of the drop. Liquid was pumped into the drop during each experiment to ensure that the drop front was advancing. The camera and microscope assembly could be moved to the right or left to allow the contact point of the advancing drop on each side to be followed. The images were taken from both sides of the drop. This feature allows measuring the right and the left contact angles separately. Any difference between the right and left contact angles could be an indication of a misalignment in the hardware and can be used as a malfunction detection feature (see below).

The highly magnified images were obtained with an interval of one image per second. Images were processed by the APF program by fitting a third-order polynomial to the first 130 pixels of the drop profile. Each run of the experiments consists of more than one hundred observations (i.e. contact angle measurement). For each liquid–solid combination several replications were produced using different samples of solid surfaces.

As an example, an experiment consisting of three runs was performed with sessile drops of

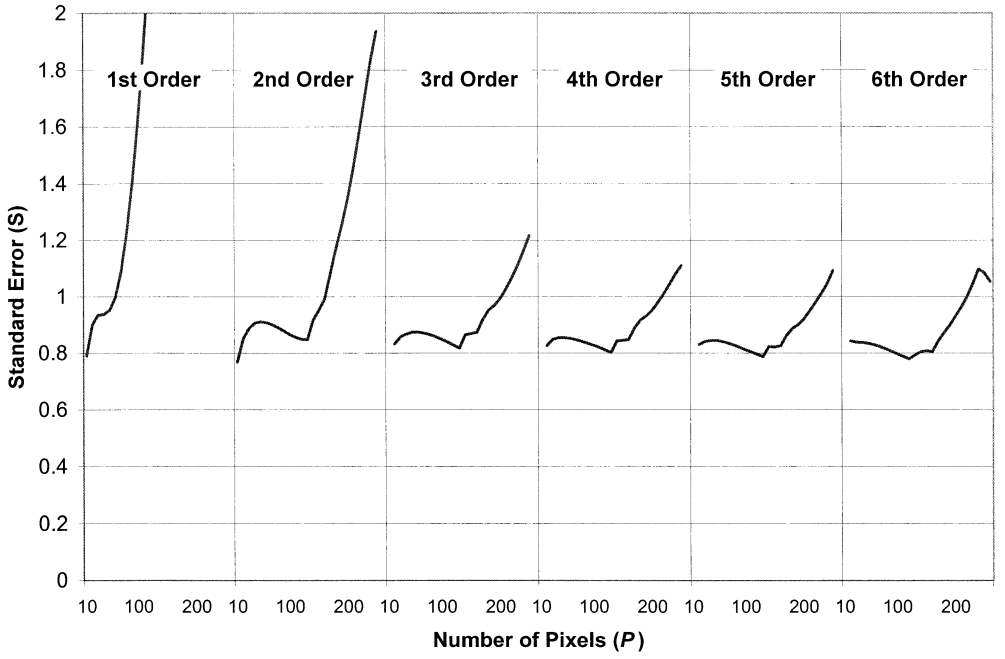

Fig. 14. Average standard error for several polynomials of different order versus number of pixels. Each of the sections between the vertical gridlines represents a different polynomial (first-order to sixth-order); and the horizontal axis shows the number of pixels (10, 20,. . .,260) used in the fitting procedure.

water on the PMMA coated surfaces. Contact angles from the left and the right side of the sessile drop were measured using the APF method. Fig. 15 illustrates the result of an experimental run.

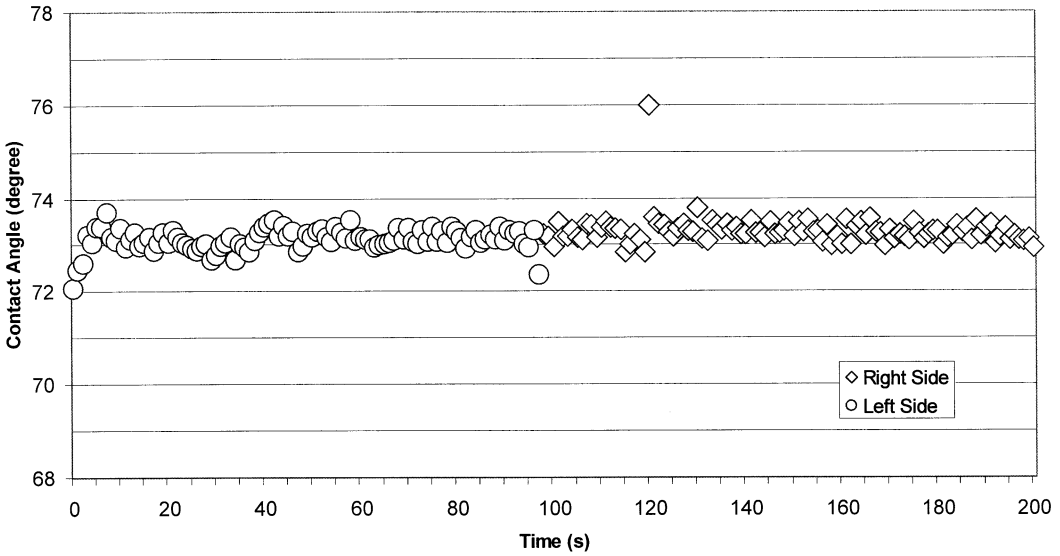

Fig. 15. Advancing contact angles of a sessile drop of water on a PMMA surface (run A of the experiment). Contact angles are calculated by the APF program using the third-order polynomial and 130 pixels.

In the APF method it is assumed that the solid surface is horizontal and the camera is vertically adjusted. Thus the contact angle is measured as the slope of the drop profile with respect to a horizontal line in the digital image. However, APF can detect any tilt in the camera or the solid surface (e.g. due to uneven thickness of the coating), by calculating the contact angles from both sides of the drop. Any tilt in the hardware setup, α, will cause an error of $+\alpha$ degrees on one side of the drop and $-\alpha$ on the other side. Thus, the right and left contact angles would be different by 2α degrees (Fig. 16). Therefore, by measuring right and left contact angles separately, one can detect potential misalignments and consequently adjust all of the observations.

Table 1 shows the average of right and left contact angles of the above experiment (water on PMMA). Data in Table 1 indicate that the right contact angle was 0.34° higher than the left contact angle. Since all three runs of this experiment were performed with the same hardware setting, it was concluded that the above difference was due to a 0.17° tilt in the hardware. To eliminate this effect, the value of 0.17 was subtracted from each of the left contact angle observations and was added to each of the right contact angles. Finally, the averages of different runs were calculated from the adjusted values, and are used to calculate the overall average (last column in Table 1).

Several experiments were performed with both ADSA and APF using different combinations of solids and liquids, i.e., decane on Teflon, decanol on Teflon, formamide on DF55 (a fluorinated film), and formamide on DF13 (a fluorinated film). Each experiment consists of several runs; the overall average was calculated using the above procedure. Table 2 compares the average contact angles of ADSA with those of APF, indicating good agreement between the two methodologies. Possible causes for minor discrepancies between the results of the two schemes are discussed below.

4. Discussion and conclusion

In general, it was found that developing a statistically sound curve fitting method for contact

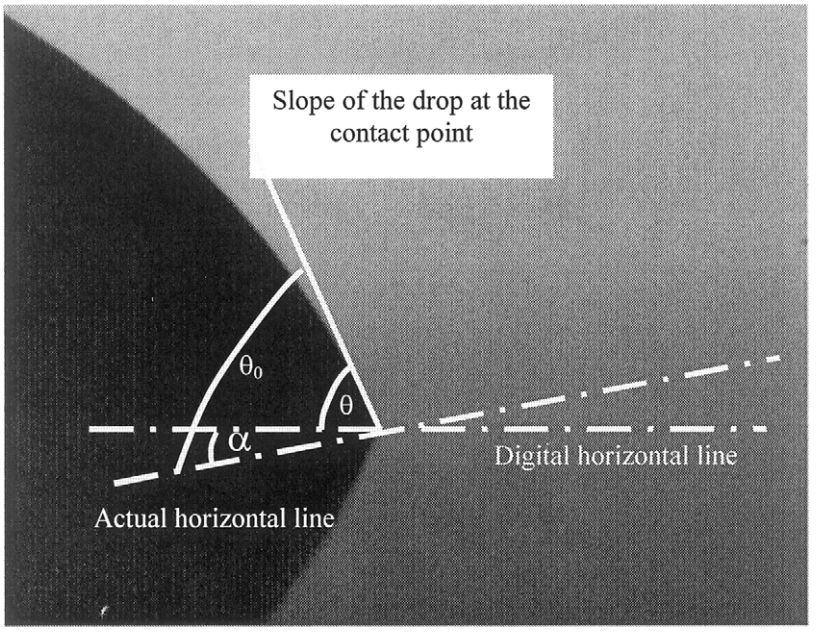

Fig. 16. The APF method measures the contact angle with respect to a digital horizontal line, i.e., a horizontal line in the digital image. If there is a tilt in the camera or the solid surface (α), the measured contact angle (θ) would be different from the real contact angle (θ_0) by α degrees.

Table 1
Contact angles of sessile drops of water on PMMA coated surfaces, measured by the APF method

Run	Left contact angle	Right contact angle	Average of each run (after adjustments)	Overall average
A	73.03	73.14	73.07	73.07
B	72.65	72.09	72.32	
C	74.09	73.51	73.81	
Average of each side	73.25	72.91		
Difference of averages	0.34			

The experiment consists of three runs (replications).

Table 2
Summary of contact angle measurements by the APF and the ADSA schemes

Experiment		Contact angle (°)	
Liquid	Solid surface	APF	ADSA
Decane	Teflon	56.92 ± 0.48	58.19 ± 0.45
Decanol	Teflon	73.29 ± 0.49	73.83 ± 0.38
Formamide	DF55	69.62 ± 0.68	68.45 ± 0.73
Formamide	DF13	88.13 ± 0.84	86.47 ± 0.96

Each contact angle represents the average of several runs and the errors are the standard deviation.

angle measurements is not a trivial task. Good agreement was found between the APF method presented in this paper and the reliable ADSA methodology. However, it was illustrated that to achieve such agreement a careful analysis is required to determine the parameters of the method, e.g., the number of pixels in the curve fitting, the order of the polynomial, and the parameters of the edge detection technique. As illustrated in Table 2, there are minor discrepancies ($< 1.5°$) between the results of the two methods, which can be explained by the following reasons.

(1) ADSA analyzes the whole drop profile assuming that the solid surface is ideal and the drop is Laplacian and axisymmetric; by comparison, APF only considers the area near the contact point and measures the macroscopic contact angle, which is the manifestation of local surface energy and topography. Thus, for real surfaces the results of ADSA and APF might be slightly different.

(2) A polynomial is not a perfect equation to describe drop profiles. Although a thorough analysis was performed to select the optimal polynomial, only the governing Laplacian curve can be fitted to a drop profile without producing an error. Therefore, part of the observed difference in the results of the method could be due to the equation that is used.

Just as the ADSA contact angles, the APF angle is a macroscopic one. However, the ADSA angle is global in the sense that it considers the whole profile, and does not give particular weight to points on the profile relatively close to the three-phase line. Thus, it tends to smooth out minor irregularities of the three-phase line close to but not in the meridian plane. This is due to the fact that, even if there are some small corrugations in the three-phase line, surface tension will quickly make the drop axisymmetric a short distance above the solid surface. By comparison, the APF angle is strictly local, reflecting nothing but the profile in the meridian plane, close to the three-phase line.

The analysis performed in this paper revealed that the image processing of highly magnified images is more difficult than regular low magnification images. For this purpose, using the LOG edge detection method with a high filtering parameter (e.g. 4.0) and a low sensitivity parameter (e.g. 0.0001) was recommended. However, circumspection is necessary to ensure that the actual drop profile is not affected by the filtering procedure. Regarding the parameters of the curve fitting module, it was shown that third-order polynomials with 130 coordinate points will produce accurate and stable contact angle results. Generally, these parameters can be used for any contact angle measurement of sessile drops. However, when

higher accuracy of the results is required or when the drop profile is different from regular sessile drops (e.g. liquid lens systems), it is recommended to repeat the analysis performed in this paper to ensure that the parameters are chosen optimally. Moreover, it should be noted that the optimum parameters obtained in this paper are based on the digital resolution of 60.4 lp/mm (Cohu CCD camera 4910 with 640×480 pixels were used for imaging). For higher resolutions the statistical procedure should be repeated to verify the validity of the parameters.

APF is an intermediate between the conventional goniometer method and the advanced ADSA methodology. APF is preferred to the goniometer method because it is not subjective and it provides higher accuracy. This approach also has the following advantages over the current versions of ADSA.

(1) No assumption (e.g. Laplacian drop, axisymmetric drop, perfect solid surface) has been made in APF. Therefore, it can be employed in various situations where ADSA is not applicable, e.g., electrically charged drops or liquid lens systems.

(2) The APF technique focuses only on the contact point of the drop and measures the contact angle with high-accuracy. Therefore the method is ideal for detecting small changes in the contact angle, and also for the study of solid surface properties (e.g. solid surface energies).

(3) Information about the density difference across the interface $\Delta\rho$, and the gravitational acceleration g is not needed for APF, so it can be applied to unknown liquids.

(4) The ADSA scheme involves advanced and complicated algorithms; however APF has simpler algorithms and it would be easier to modify the scheme to be applicable to other situations, not only sessile drops.

Acknowledgements

This investigation was financially supported by the Canadian Space Agency (contract no: 9F007-006051/001/ST) (AWN and AA) and a University of Toronto Open Fellowship (AB).

References

[1] T. Young, Phil. Trans. R. Soc. Lond. 95 (1805) 65.
[2] A.W. Neumann, in: J.F. Padday (Ed.), Wetting, Spreading and Adhesion, Academic Press, New York, 1978, p. 3.
[3] R.J. Good, in: R.J. Good, R.R. Stromberg (Eds.), Surface and Colloid Science, vol. 11, Plenum Press, New York,, 1979, p. 1.
[4] A. Marmur, Adv. Colloid Interface Sci. 19 (1983) 75.
[5] G. Wolansky, A. Marmur, Langmuir 14 (1998) 5292.
[6] C.N.C. Lam, J.Y. Lu, A.W. Neumann, Measuring Contact Angle, in: K. Holmberg, M.J. Schwuger, D.O. Shah (Eds.), Handbook of Applied Surface and Colloid Chemistry, Part 5: Analysis in Surfact Chemistry, Wiley Europe 2001.
[7] A. Amirfazli, S. Hanig, A. Müller, A.W. Neumann, Langmuir 16 (2000) 2024.
[8] A. Marmur, J. Colloid Interface Sci. 186 (1997) 462.
[9] D.K. Kwok, T. Gietzelt, K. Grundke, H.-J. Jacobasch, A.W. Neumann, Langmuir 13 (1997) 2880.
[10] A.W. Zisman, Contact angle, wettability and adhesion, in: Advances in Chemistry Series, vol. 43, American Chemical Society, Washington DC, 1964.
[11] F.M. Fowkes, Ind. Eng. Chem. 12 (1964) 40.
[12] O. Driedger, A.W. Neumann, P.J. Sell, Kolloid-Z. Z. Polym. 201 (1965) 52.
[13] A.W. Neumann, R.J. Good, C.J. Hope, M. Sejpal, J. Colloid Interface Sci. 49 (1974) 291.
[14] J.K. Spelt, D. Li, The equation of state approach to interfacial tensions, in: A.W. Neumann, J.K. Spelt (Eds.), Applied Surface Thermodynamics, Marcel Dekker, New York, 1996, p. 239.
[15] C.H. Byers, A. Amaranth, Chem. Eng. Prog. (1995) 63.
[16] Hayati, A.I. Bailey, T.F. Tadros, J. Colloid Interface Sci. 117 (1987) 205.
[17] T.G. Twardeck, IBM J. Res. Dev. 21 (1977) 31.
[18] Y.A. Shchipunov, A.F. Kolpukou, Adv. Colloid Interface Sci. 35 (1991) 331.
[19] M.T. Harris, T.C. Scott, O.A. Basaran, C.H. Byers, Mater. Res. Soc. Symp. Proc. 180 (1990) 853.
[20] A.W. Neumann, R.J. Good, in: R.J. Good, R.R. Stromberg (Eds.), Surface and Colloid Science, vol. 11, Plenum Press, New York, 1979, p. 31.
[21] Y. Rotenberg, L. Boruvka, A.W. Neumann, J. Colloid Interface Sci. 93 (1983) 169.
[22] P. Cheng, D. Li, L. Boruvka, Y. Rotenberg, A.W. Neumann, Colloids Surf. 93 (1983) 169.
[23] S. Lahooti, O.I. del Río, P. Cheng, A.W. Neumann, Axisymmetric drop shape analysis, in: A.W. Neumann, J.K. Spelt (Eds.), Applied Surface Thermodynamics, Marcel Dekker, New York, 1996, p. 441.
[24] D.Y. Kwok, R. Lin, M. Mui, A.W. Neumann, Colloids Surf. A 116 (1996) 63.
[25] O.I. del Río, D.Y. Kwok, R. Wu, J.M. Alvarez, A.W. Neumann, Colloids Surf. A 143 (1998) 197.
[26] S.M. Alvarez, A. Amirfazli, A.W. Neumann, Colloids Surf. A 156 (1999) 163.

[27] J.K. Spelt, E.I. Vargha-Butlen, in: A.W. Neumann, J.K. Spelt (Eds.), Applied Surface Thermodynamics, Marcel Dekker, New York, 1996, p. 379.
[28] A.W. Adams, A.P. Gast, Physical Chemistry of Surfaces, sixth ed., Wiley, New York, 1998.
[29] A. Amirfazli, J. Graham-Eagle, S. Pennell, A.W. Neumann, Colloids Surf. A 161 (2000) 63.
[30] A.S. Dimitrov, P.A. Kralchevsky, A.D. Nikolov, H. Noshi, M. Matsumoto, J. Colloid Interface Sci. 145 (1991) 279.
[31] P. Chen, S.S. Susnar, A. Amirfazli, C. Mak, A.W. Neumann, Langmuir 13 (1997) 3035.
[32] M.L. James, G.M. Smith, J.C. Wolford, Applied Numerical Methods for Digital Computation, Harper Collins College Publishers, New York, 1993, p. 315.